Sound propagation in a turbulent atmosphere near the ground: A parabolic equation approach

Vladimir E. Ostashev[a)]
NOAA/Environmental Technology Laboratory, 325 Broadway, Boulder, Colorado 80305 and Physics Department, New Mexico State University, Las Cruces, New Mexico 88003

Erik M. Salomons
TNO Institute of Applied Physics, P.O. Box 155, 2600 AD Delft, The Netherlands

Steven F. Clifford and Richard J. Lataitis
NOAA/Environmental Technology Laboratory, 325 Broadway, Boulder, Colorado 80305

D. Keith Wilson
U.S. Army Research Laboratory, 2800 Powder Mill Road, Adelphi, Maryland 20783-1197

Philippe Blanc-Benon and Daniel Juvé
Centre Acoustique, équipe LMFA/UMR CNRS 5509, Ecole Centrale de Lyon, 36 Avenue Guy de Collongue, BP 163, 69131 Ecully, France

(Received 3 September 1999; accepted for publication 3 January 2001)

The interference of the direct wave from the point source to the receiver and the wave reflected from the impedance ground in a turbulent atmosphere is studied. A parabolic equation approach for calculating the sound pressure p at the receiver is formulated. Then, the parabolic equation is solved by the Rytov method yielding expressions for the complex phases of direct and ground-reflected waves. Using these expressions, a formula for the mean squared sound pressure $\langle|p|^2\rangle$ is derived for the case of anisotropic spectra of temperature and wind velocity fluctuations. This formula contains the ''coherence factor,'' which characterizes the coherence between direct and ground-reflected waves. It is shown that the coherence factor is equal to the normalized coherence function of a spherical sound wave for line-of-sight propagation. For the case of isotropic turbulence, this result allows one to obtain analytical formulas for $\langle|p|^2\rangle$ for the Kolmogorov, Gaussian, and von Karman spectra of temperature and wind velocity fluctuations. Using these formulas, the effects of temperature and wind velocity fluctuations, and the effects of different spectra of these fluctuations on the mean squared sound pressure, are numerically studied. Also the effect of turbulent anisotropy on the interference of direct and ground reflected waves is numerically studied. Finally, it is shown that the mean squared sound pressure $\langle|p|^2\rangle$ calculated for the von Karman spectrum of temperature fluctuations agrees well with experimental data obtained in a laboratory experiment. © *2001 Acoustical Society of America.* [DOI: 10.1121/1.1356022]

PACS numbers: 43.28.Fp, 43.20.Bi, 43.20.Fn [LCS]

I. INTRODUCTION

For many problems of atmospheric acoustics, a sound field p is the sum of the direct wave from the source to the receiver and that reflected from the ground; see Fig. 1. The interference between these waves results in the interference maxima and minima of p. Quite often, the source and receiver are close to the ground while the horizontal distance between them is in the range from several tens to several hundred meters. In this case, the amplitude of the sound field p can be very small at interference minima in the absence of atmospheric turbulence. But turbulence is always present in the atmosphere. It results in random fluctuations in phase and amplitude of the direct and ground-reflected waves, and partial or complete destruction of the coherence between these waves. This destruction can cause an increase of the mean squared sound pressure $\langle|p|^2\rangle$ at the interference minima by tens of dB. The most recent theory of this phenomenon has been developed by Clifford and Lataitis,[1] who had generalized the results of previous research; e.g., see Ref. 2 and the references presented there.

Clifford and Lataitis used the Rytov method to calculate phase and log-amplitude fluctuations of the direct and ground-reflected waves due to refractive index fluctuations. They followed Tatarskii,[3] who considered the case when refractive index fluctuations are caused by temperature fluctuations. Furthermore, Clifford and Lataitis calculated $\langle|p|^2\rangle$ by an energy-conserving approach. Finally, they presented a formula for $\langle|p|^2\rangle$ for a Gaussian correlation function of refractive index fluctuations. These results made a significant contribution to the development of atmospheric acoustics and have been used by many specialists in the field.

Since the publication of the Clifford and Lataitis paper,[1] atmospheric acoustics has been developed significantly. It has become clear, e.g., Refs. 4, 5, that the effects of wind velocity fluctuations on the statistical moments of a sound field are usually greater than the effects of temperature fluctuations. Furthermore, while the Gaussian spectrum of turbu-

a)Electronic mail: vostashe@nmsu.edu

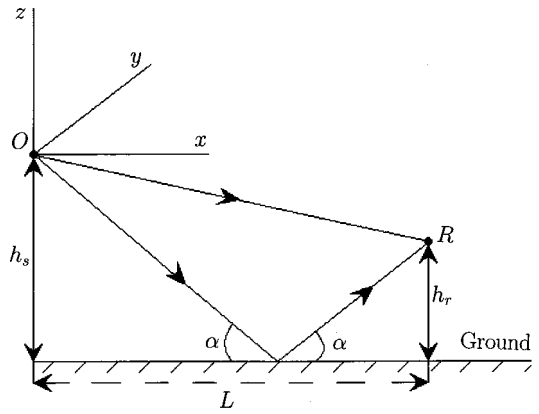

FIG. 1. The geometry of the problem. The source is located at the origin O of the coordinate system x, y, z, and the receiver is located at the point R. Line segments with arrows indicate directions of propagation of the direct and ground-reflected waves. Source and receiver heights above the ground are h_s and h_r, and the horizontal distance between them is L.

lence was widely used in atmospheric acoustics in the 1970s and 1980s, nowadays the more realistic Kolmogorov and von Karman spectra are employed, e.g., Refs. 4, 6. It has also been shown[5,7] that anisotropy of atmospheric turbulence may significantly affect the statistical moments of a sound field. Finally, the parabolic equation method has been used for analytical and numerical calculations of the statistical moments of a sound field, e.g., Refs. 4, 8, 9, 10.

The goal of our current research is to generalize the Clifford and Lataitis theory[1] by taking into account the aforementioned developments in atmospheric acoustics. In this paper, sound propagation over the impedance ground in the atmosphere with both temperature and velocity fluctuations is described on the basis of the parabolic equation. The Rytov method is used to approximately solve the parabolic equation and derive an equation for $\langle|p|^2\rangle$, which is valid for anisotropic spectra of temperature and velocity fluctuations. Then, we derive formulas for $\langle|p|^2\rangle$ for isotropic turbulence with the Kolmogorov, Gaussian, and von Karman spectra of temperature and velocity fluctuations. Furthermore, we numerically study the effects of temperature and velocity fluctuations, the effects of different spectra of turbulence, and the effects of turbulent anisotropy on $\langle|p|^2\rangle$. Finally, we show that the theoretical results for $\langle|p|^2\rangle$ for the von Karman spectrum of temperature fluctuations are in a good agreement with experimental data obtained in a large anechoic chamber in Ecole Centrale de Lyon.

Preliminary reports on a generalization of the Clifford and Lataitis theory[1] were simultaneously and independently presented at the 8th International Symposium on Long Range Sound Propagation.[11,12] These presentations gave two different approaches for the problem: a parabolic equation approach,[11] and an approach based on the spectral representation of refractive-index fluctuations.[12] The collaborative effort toward further development of these approaches resulted in two papers: the present paper and the companion one.[13] The papers complement each other, and explain the connection between results obtained by these approaches.

The paper is organized as follows. In Sec. I, the basic equations of the parabolic equation approach are presented. In Sec. II, expressions for $\langle|p|^2\rangle$ are derived. In Sec. III, the interference of the direct and ground-reflected waves in a turbulent atmosphere is studied numerically; furthermore, some of theoretical results obtained are compared with experimental data. And in Sec. V, the results obtained are summarized.

II. BASIC EQUATIONS

A. Geometry of the problem

Figure 1 shows the geometry of the problem, with a source and receiver in a turbulent atmosphere near an impedance ground surface. The source and receiver heights above the ground are h_s and h_r, respectively. The horizontal distance between them is L. The path length of the wave from the source to the receiver is given by $R_s=\sqrt{L^2+(h_s-h_r)^2}$, and that of the wave reflected from the ground is $R_i=\sqrt{L^2+(h_s+h_r)^2}$. The source is located at the origin of the Cartesian coordinate system x, y, z. The z-axis is directed upward, and the x-axis is in the horizontal direction from source to receiver. The ground surface coincides with the horizontal plane $z=-h_s$. The mean value of temperature T is constant and is equal to T_0, and the mean value of the wind velocity vector $\mathbf{v}$ is zero.

In the absence of atmospheric turbulence, the sound pressure p at the receiver is the sum of the sound fields of the direct and ground-reflected waves (e.g., Refs. 14, 15):

$$p=p_s^{(0)}+p_i^{(0)}=\frac{\exp(ikR_s)}{R_s}+Q\frac{\exp(ikR_i)}{R_i}. \tag{1}$$

Here, $p_s^{(0)}$ and $p_i^{(0)}$ correspond to the direct and reflected waves, the time-dependence of p is omitted, k is the sound wavenumber, and Q is the spherical-wave reflection coefficient which can also be interpreted as the apparent strength of the image source. For the locally reacting surface and in the approximation of near-grazing sound propagation when $R_s\sim R_i\gg h_s,h_r$, the coefficient Q is given by

$$Q=\frac{\sin\alpha-\beta+2\beta[1+i\sqrt{\pi}de^{-d^2}\operatorname{erfc}(-id)]}{\sin\alpha+\beta}. \tag{2}$$

Here, β is the admittance of the surface, α is the grazing angle of the wave incident on the ground (see Fig. 1), $\operatorname{erfc}(x)=(2/\sqrt{\pi})\int_x^\infty\exp(-t^2)dt$ is the complementary error function, and $d=\sqrt{ikR_i/2}[\beta+(h_s+h_r)/R_i]$ is the numerical distance. The range of applicability of Eq. (2) for Q is studied in detail in Refs. 14, 15, 16.

Due to fluctuations in the temperature $\tilde{T}(\mathbf{R})$ and velocity $\mathbf{v}(\mathbf{R})$ in the atmosphere, where $\mathbf{R}=(x,y,z)$, the sound field p becomes a random field. In many applications, it is important to know the mean squared sound pressure $\langle|p|^2\rangle$, where $\langle\,\rangle$ denotes an ensemble average.

B. Reformulation of the geometry of the problem

The impedance ground located at $z=-h_s$ complicates significantly the calculation of $\langle|p|^2\rangle$. This calculation would be simpler in a free space. Our main idea is that calculation of $\langle|p|^2\rangle$ over the impedance ground can be approximately

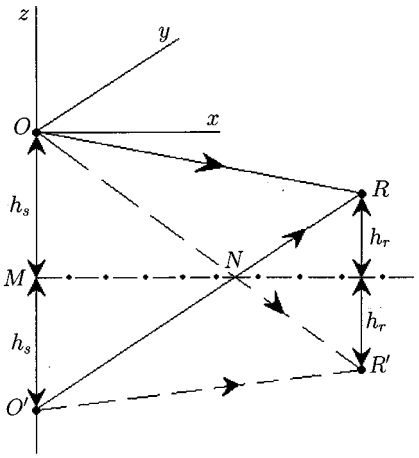

FIG. 2. The new geometry of the problem which includes the image source. Source, image source, receiver, and image receiver are located at the points O, O', R, and R', respectively. The ground is being removed, and a random medium is filling the whole space. The dash–dotted line coincides with the surface of the ground in the geometry of Fig. 1. Line segments with arrows indicate directions of propagation of different waves from the source and the image source.

replaced by the calculation for the geometry shown in Fig. 2. In this geometry, the ground is removed, the random medium fills the whole space and is symmetrical with respect to the plane $z=-h_s$, and the source at the point $\mathbf{R}_s=(0,0,0)$ is supplemented by an image source of the strength Q located at the point $\mathbf{R}_i=(0,0,-2h_s)$.

We now give a mathematical formulation of the problem, the geometry of which is shown in Fig. 2. If the random fields $\tilde{T}$ and $\mathbf{v}$ are relatively weak, the sound pressure p due to the source and image source can be sought as a solution of the parabolic equation:[4]

$$2ik\frac{\partial p}{\partial x}+\Delta_\perp p+2k^2\left(1+\frac{\mu_{\mathrm{mov}}}{2}\right)p=0, \tag{3}$$

where $\Delta_\perp=(\partial^2/\partial y^2)+(\partial^2/\partial z^2)$, and $\mu(\mathbf{R})$ describes the random medium in the geometry of Fig. 2. $\mu(\mathbf{R})$ can be expressed in the following form:

$$\mu(x,y,z)=\Theta(z+h_s)\epsilon_{\mathrm{mov}}(x,y,z)+[1-\Theta(z+h_s)]\epsilon_{\mathrm{mov}}(x,y,-z-2h_s). \tag{4}$$

Here, $\Theta(z)=1$ if $z\geqslant 0$, $\Theta(z)=0$ if $z<0$, and $\epsilon_{\mathrm{mov}}(\mathbf{R})=-\tilde{T}(\mathbf{R})/T_0-2v_x(\mathbf{R})/c_0$ is twice the fluctuations in the acoustic refractive index in a moving atmosphere in the geometry of Fig. 1, where v_x is the fluctuations of the wind velocity component in the x-direction, and c_0 is the mean value of the adiabatic sound speed. It follows from Eq. (4) that the random field $\mu=\epsilon$ above the plane $z=-h_s$ and is symmetrical with respect to this plane. We assume that the random field ϵ_{mov} has a Gaussian distribution, $\langle\epsilon_{\mathrm{mov}}\rangle=0$, and that $\tilde{T}$ and $\mathbf{v}$ are uncorrelated. The latter assumption is valid for isotropic turbulence.[3]

The initial condition to the parabolic equation (3) is formulated in the plane $x=0$:

$$p(x=0,\mathbf{r})=\frac{2\pi i}{k}\delta(\mathbf{r}-\mathbf{r}_s)+\frac{2\pi iQ}{k}\delta(\mathbf{r}-\mathbf{r}_i), \tag{5}$$

where $\mathbf{r}=(y,z)$ are the transverse coordinates, $\mathbf{r}_s=(0,0)$, $\mathbf{r}_i=(0,-2h_s)$, and $\delta(\mathbf{r})$ is the delta-function. The first term on the right-hand side of Eq. (5) corresponds to the point source located at $\mathbf{R}_s=(0,0,0)$, while the second term corresponds to the image source of the strength Q located at $\mathbf{R}_i=(0,0,-2h_s)$.

In the limiting case $\epsilon_{\mathrm{mov}}=0$, the parabolic equation (3) with the initial condition (5) can be easily solved. The result is

$$p(x,\mathbf{r})=p_s^{(0)}+p_i^{(0)}=\frac{\exp\left(ikx+\dfrac{ik(\mathbf{r}-\mathbf{r}_s)^2}{2x}\right)}{x}+Q\frac{\exp\left(ikx+\dfrac{ik(\mathbf{r}-\mathbf{r}_i)^2}{2x}\right)}{x}, \tag{6}$$

where $p_s^{(0)}$ and $p_i^{(0)}$ are the fields of the waves from the source and image source to the receiver. This formula for p coincides with Eq. (1) in the approximation of near-grazing sound propagation.

The parabolic equation (3) with the initial condition (5) and the random field $\mu(\mathbf{R})$ given by Eq. (4) are the starting equations of our approach for calculating $\langle|p|^2\rangle$. Other statistical moments of a sound field can also be calculated on the basis of Eqs. (3)–(5). It is shown in Appendix A that, when calculating p, the new geometry of the problem shown in Fig. 2 is equivalent to the original one in Fig. 1 if $Q=1$. It is also shown in Appendix A that, for $Q=1$, both geometries are equivalent to the geometry in Ref. 13. The latter geometry is similar to that in Fig. 2; however, instead of the image source, an image receiver is used. Since in the limiting case $\epsilon_{\mathrm{mov}}=0$, Eqs. (3)–(5) correctly describe sound propagation near the impedance ground, we expect that they can be used to approximately describe sound propagation if the atmospheric turbulence is relatively weak. The main advantage of the geometry in Fig. 2 is that the parabolic equation (3) allows us to use various methods for calculating $\langle|p|^2\rangle$ and other statistical moments of the sound field, namely, geometrical acoustics, Rytov method, Markov approximation, Feynman path-integral technique, diagram technique, etc. These methods are well developed in theories of wave propagation in unbounded random media.[3,4,17,18] Note that in the theories of waves in random media, an approach for calculating the statistical moments of a field p which satisfies Eq. (3) is usually called the parabolic equation approach or method, e.g., see Refs. 4, 17, 18.

III. RYTOV METHOD

A. Mean squared sound pressure

For the geometry in Fig. 2, the sound field p at the receiver is the sum of the field due to the source and the field due to the image source: $p(\mathbf{R})=p_s(\mathbf{R})+p_i(\mathbf{R})$, where the subscripts s and i stand for source and image source. Sound waves from both sources exhibit phase and amplitude fluctuations in the random medium. Following the Rytov method, we express p_s and p_i in the forms $p_s=p_s^{(0)}e^{\psi_s}$ and $p_i=p_i^{(0)}e^{\psi_i}$. Here, $p_s^{(0)}$ and $p_i^{(0)}$ are the sound fields in an

atmosphere without random inhomogeneities and are given by the first and second terms in Eq. (6) [or in Eq. (1)], respectively. Furthermore, $\psi_s=\chi_s+iS_s$ are fluctuations in the complex phase of the wave emitted by the source, and $\psi_i=\chi_i+iS_i$ are those in the wave emitted by the image source, where χ and S with the corresponding indexes are fluctuations in the log-amplitude and phase of these waves. Thus, the Rytov method allows us to express the sound field p at the receiver in the form

$$p(\mathbf{R})=p_s^{(0)}(\mathbf{R})e^{\psi_s(\mathbf{R})}+p_i^{(0)}(\mathbf{R})e^{\psi_i(\mathbf{R})}. \tag{7}$$

Using the Rytov method, χ_j and S_j can be expressed as a series in ϵ_{mov}: $\chi_j=O(\epsilon_{\mathrm{mov}})+O(\epsilon_{\mathrm{mov}}^2)+\cdots$, and $S_j=O(\epsilon_{\mathrm{mov}})+O(\epsilon_{\mathrm{mov}}^2)+\cdots$. Hereinafter, the subscript j stands for s or i. It can be shown from these series that χ_j and S_j have Gaussian distributions, and that

$$\begin{aligned}\overline{\chi_j}&=O(\langle\epsilon_{\mathrm{mov}}^2\rangle)+O(\langle\epsilon_{\mathrm{mov}}^4\rangle)+\cdots,\\ \overline{S_j}&=O(\langle\epsilon_{\mathrm{mov}}^2\rangle)+O(\langle\epsilon_{\mathrm{mov}}^4\rangle)+\cdots.\end{aligned} \tag{8}$$

Furthermore, $\langle\chi_j^2\rangle$ and $\langle S_j^2\rangle$ can also be expressed as series in even powers of $\langle\epsilon_{\mathrm{mov}}^2\rangle$, analogous to series (8). In the derivations below, we keep terms of order $\langle\epsilon_{\mathrm{mov}}^2\rangle$ and neglect those proportional to $\langle\epsilon_{\mathrm{mov}}^4\rangle$.

Substituting the values of $p_s^{(0)}$ and $p_i^{(0)}$ from Eq. (1) into Eq. (7), squaring both sides of the resulting formula, and performing ensemble averaging, one obtains the formula for the mean squared sound pressure:

$$\begin{aligned}\langle|p|^2\rangle=&\frac{1}{R_s^2}\langle e^{\psi_s+\psi_s^*}\rangle+\frac{|Q|^2}{R_i^2}\langle e^{\psi_i+\psi_i^*}\rangle\\ &+\frac{|Q|}{R_sR_i}[e^{i\Omega}\langle e^{\psi_s^*+\psi_i}\rangle+e^{-i\Omega}\langle e^{\psi_s+\psi_i^*}\rangle],\end{aligned} \tag{9}$$

where $Q=|Q|e^{i\Omega}$. In Eq. (9), $\langle e^{\psi_s+\psi_s^*}\rangle=\langle e^{\psi_i+\psi_i^*}\rangle=1$. These equalities are consequences of the energy conservation in the parabolic equation approximation.[1,17] The calculation of the terms $\langle e^{\psi_s^*+\psi_i}\rangle$ and $\langle e^{\psi_s+\psi_i^*}\rangle$ in Eq. (9) is presented in Appendix B. Substitution of these terms into Eq. (9) yields

$$\begin{aligned}\langle|p|^2\rangle=&\frac{1}{R_s^2}+\frac{|Q|^2}{R_i^2}+\frac{2|Q|C}{R_sR_i}\cos[(R_i-R_s)k+\Omega\\ &+\langle\chi_sS_i\rangle-\langle\chi_iS_s\rangle+O(\langle\epsilon_{\mathrm{mov}}^4\rangle)].\end{aligned} \tag{10}$$

Here, the ''coherence'' factor C describes the coherence between the wave emitted by source and that emitted by image source, and is given by

$$\begin{aligned}C=\exp[&\langle\chi_s\chi_i\rangle+\langle S_sS_i\rangle-\tfrac{1}{2}(\langle\chi_s^2\rangle+\langle\chi_i^2\rangle+\langle S_s^2\rangle+\langle S_i^2\rangle)\\ &+O(\langle\epsilon_{\mathrm{mov}}^4\rangle)].\end{aligned} \tag{11}$$

In the case $Q=1$, Eqs. (10) and (11) are equivalent to Eqs. (6) and (7) from Ref. 13. Equations (10) and (11) differ from analogous equations in Ref. 1 only by the term $\langle\chi_iS_i\rangle-\langle\chi_sS_s\rangle$ in the argument of the cosine, which is present in Ref. 1 and is not present in Eq. (10). The reason for this difference is explained in Appendix B. This small difference does not affect the final result since in the Rytov approximation the term $\langle\chi_iS_i\rangle-\langle\chi_sS_s\rangle$ can be omitted.

B. Log-amplitude and phase fluctuations

To obtain the values of χ_s, χ_i, S_s, and S_i in Eqs. (10) and (11), we substitute $p_j=p_j^{(0)}e^{\psi_j}$ into Eq. (3) and use the first Rytov approximation for ψ_j. The result is (e.g., Ref. 19)

$$\begin{aligned}\psi_j(x,\mathbf{r})=&\frac{k^2}{4\pi}\int_0^x dx'\int_{-\infty}^{\infty}dy'\int_{-\infty}^{\infty}dz'\,\mu(x',\mathbf{r}')\\ &\times\frac{\exp\left[ik(x-x')+\dfrac{ik(\mathbf{r}-\mathbf{r}')^2}{2(x-x')}\right]}{x-x'}\frac{p_j^{(0)}(x',\mathbf{r}')}{p_j^{(0)}(x,\mathbf{r})}.\end{aligned} \tag{12}$$

We now rewrite formula (12) for the wave emitted by source and that emitted by the image source. For both waves, we have $x=L$, and $\mathbf{r}=(0,h_r-h_s)$. We also take into account that μ is given by Eq. (4). Substituting $p_s^{(0)}$ from Eq. (6) into Eq. (12), one obtains the complex amplitude of the wave emitted by the source:

$$\begin{aligned}\psi_s=&\frac{k^2L}{4\pi}\int_0^L\frac{dx}{x(L-x)}\int_{-\infty}^{\infty}dy\left[\int_{-h_s}^{\infty}dz\,\epsilon_{\mathrm{mov}}(x,y,z)\right.\\ &\left.+\int_{-\infty}^{-h_s}dz\,\epsilon_{\mathrm{mov}}(x,y,-z-2h_s)\right]\\ &\times\exp\left\{\frac{ikL[y^2+(z+(h_s-h_r)x/L)^2]}{2x(L-x)}\right\}.\end{aligned} \tag{13}$$

Substituting $p_i^{(0)}$ from Eq. (6) into Eq. (12), one obtains the complex amplitude ψ_i of the wave emitted by the image source. It is worthwhile to express ψ_i as a sum of two terms corresponding to two terms in Eq. (4): $\psi_i=\psi_1+\psi_2$, where

$$\begin{aligned}\psi_1=&\frac{k^2L}{4\pi}\int_0^L\frac{dx}{x(L-x)}\int_{-\infty}^{\infty}dy\int_{-\infty}^{-h_s}dz\,\epsilon_{\mathrm{mov}}(x,y,-z-2h_s)\\ &\times\exp\left\{\frac{ikL[y^2+(z+2h_s-(h_s+h_r)x/L)^2]}{2x(L-x)}\right\},\end{aligned} \tag{14}$$

$$\begin{aligned}\psi_2=&\frac{k^2L}{4\pi}\int_0^L\frac{dx}{x(L-x)}\int_{-\infty}^{\infty}dy\int_{-h_s}^{\infty}dz\,\epsilon_{\mathrm{mov}}(x,y,z)\\ &\times\exp\left\{\frac{ikL[y^2+(z+2h_s-(h_s+h_r)x/L)^2]}{2x(L-x)}\right\}.\end{aligned} \tag{15}$$

In Eqs. (13)–(15) for ψ_s and ψ_i, the limits of integration over y and z are from $-\infty$ to ∞. However, integration volumes can be much narrower. Indeed, it is well known[17] that in the geometrical acoustics approximation the statistical moments of phase and log-amplitude fluctuations are given by an integral along the path of the wave from source to receiver, with the integrand proportional to the correlation function of random inhomogeneities in a medium. In the geometry in Fig. 2, there are two such paths, OR and $O'R$. Therefore, the volumes essential for integration in Eqs. (13)–(15) are the tubes along OR and $O'R$, with transverse scales of order l, where l is a scale of the correlation function of medium inhomogeneities. Note that the geometrical acoustics approximation is valid if the wave parameter $D=L/(kl^2)$ is much less than 1.

Let us simplify Eqs. (13)–(15) in this approximation. Hereinafter, we assume that $l \ll h_s, h_r$. In this case, the integration volumes along OR and $O'R$ are relatively thin tubes with respect to h_s, h_r, and L. Furthermore, the integration volume along OR is always located in the region $z > -h_s$. Therefore, the second term in the square brackets in Eq. (13) can be neglected, and the formula for the complex phase ψ_s is simplified:

$$\psi_s = \frac{k^2 L}{4\pi} \int_0^L \frac{dx}{x(L-x)} \int_{-\infty}^{\infty} dy \int_{-h_s}^{\infty} dz\, \epsilon_{\mathrm{mov}}(x,y,z) \times \exp\left\{ \frac{ikL[y^2 + (z + (h_s - h_r)x/L)^2]}{2x(L-x)} \right\}. \quad (16)$$

The integration volume along $O'R$ can be split into two volumes. The first one is along the line segment $O'N$, and the second one is along the line segment NR (see Fig. 2). These two integration volumes correspond to ψ_1 and ψ_2. Since the integration volume along $O'N$ is relatively thin, the limits of integration over x in Eq. (14) for ψ_1 can be taken from 0 to L_1, where $L_1 = L/(h_r/h_s + 1)$ is the length of the line segment MN. Introducing a new integration variable $z' = -z - 2h_s$ in Eq. (14) and then denoting $z' = z$, one obtains

$$\psi_1 = \frac{k^2 L}{4\pi} \int_0^{L_1} dx \int_{-\infty}^{\infty} dy \int_{-h_s}^{\infty} dz\, \frac{\epsilon_{\mathrm{mov}}(x,\mathbf{r})}{x(L-x)} \times \exp\left\{ \frac{ikL[y^2 + (z + (h_s + h_r)x/L)^2]}{2x(L-x)} \right\}. \quad (17)$$

Analogously, the lower limit of integration in Eq. (15) can be approximately replaced by L_1:

$$\psi_2 = \frac{k^2 L}{4\pi} \int_{L_1}^{L} dx \int_{-\infty}^{\infty} dy \int_{-h_s}^{\infty} dz\, \frac{\epsilon_{\mathrm{mov}}(x,\mathbf{r})}{x(L-x)} \times \exp\left\{ \frac{ikL[y^2 + (z + 2h_s - (h_s + h_r)x/L)^2]}{2x(L-x)} \right\}. \quad (18)$$

Now consider the opposite limiting case of Fraunhofer diffraction when $D \gg 1$. In this case, the volumes essential for integration in Eqs. (13)–(15) are again the tubes along OR and $O'R$ but their transverse scales are of order $\sqrt{x/k}$ and are much greater than l, at least for $x \sim L$. Nevertheless, the integration volume along OR is still located in the region $z > -h_s$ if $h_0 > \sqrt{L/k}$. Here, for simplicity, we assume that source and receiver are at the same height above the ground, and denote $h_0 = h_s = h_r$. In this case, Eq. (16) is a good approximation for ψ_s. For the considered case $D \gg 1$, it can be analogously shown that ψ_1 and ψ_2 can be approximated by Eqs. (17) and (18) if $h_0 > \sqrt{L/k}$.

If velocity fluctuations are zero, Eqs. (16)–(18) coincide with the equations for ψ_s and ψ_i presented in Ref. 1. Our derivation clearly shows which terms are neglected when deriving these equations.

C. Derivation of a formula for the coherence factor *C*

Equations (16)–(18) for ψ_s and $\psi_i = \psi_1 + \psi_2$ will be used to calculate the statistical moments in Eqs. (10) and (11). Note that in Eqs. (10) and (11), $\chi_s = \mathrm{Re}\,\psi_s$; $S_s = \mathrm{Im}\,\psi_s$; $\chi_i = \mathrm{Re}\,\psi_i = \mathrm{Re}\,\psi_1 + \mathrm{Re}\,\psi_2 = \chi_1 + \chi_2$; and $S_i = \mathrm{Im}\,\psi_i = \mathrm{Im}\,\psi_1 + \mathrm{Im}\,\psi_2 = S_1 + S_2$. Here, $\chi_1 = \mathrm{Re}\,\psi_1$, $\chi_2 = \mathrm{Re}\,\psi_2$, $S_1 = \mathrm{Im}\,\psi_1$, and $S_2 = \mathrm{Im}\,\psi_2$.

With these notations, and taking into account that ψ_1 and ψ_2 have a negligible correlation, one obtains the following formula for the coherence factor C:

$$C = \exp[\langle \chi_s \chi_1 \rangle + \langle S_s S_1 \rangle + \langle \chi_s \chi_2 \rangle + \langle S_s S_2 \rangle - \tfrac{1}{2}[\langle \chi_s^2 \rangle + \langle S_s^2 \rangle + \langle \chi_1^2 \rangle + \langle S_1^2 \rangle + \langle \chi_2^2 \rangle + \langle S_2^2 \rangle] + O(\langle \epsilon_{\mathrm{mov}}^4 \rangle)]. \quad (19)$$

Calculations of the statistical moments in Eq. (19) are straightforward but involved. The result is simpler when the statistical moments are grouped in pairs. The derivation of the expression for a sum $\langle \chi_s \chi_2 \rangle + \langle S_s S_2 \rangle$ is presented in Appendix C. The derivation is similar but not identical to the derivation in Ref. 1, where the case of isotropic turbulence is considered. The derivation of expressions for other pairs of the statistical moments in Eq. (19) are analogous to that in Appendix C. As a result, one obtains the following formulas for pairs of the statistical moments in Eq. (19):

$$\langle \chi_s \chi_1 \rangle + \langle S_s S_1 \rangle = \frac{k^2 L}{16 h_r} \int_0^{2h_r L_1/L} dz\, b_{\mathrm{eff}}(0,z) + \frac{k^2}{8\pi} \int_0^{L_1} dx \left[\int_{-\infty}^{-2xh_r/L} d\xi\, \frac{\sin\left(\frac{\xi kL(\xi/2 - m_1)}{x(L-x)} \right)}{\xi} b_{\mathrm{eff}}(0, \xi + 2h_r x/L) - \int_{-2xh_r/L}^{\infty} d\xi\, \frac{\sin\left(\frac{\xi kL(\xi/2 + m_2)}{x(L-x)} \right)}{\xi} b_{\mathrm{eff}}(0, \xi + 2h_r x/L) \right], \quad (20)$$

$$\langle \chi_s \chi_2 \rangle + \langle S_s S_2 \rangle = \frac{k^2 L}{16 h_s} \int_0^{2h_s(1 - L_1/L)} dz\, b_{\mathrm{eff}}(0,z) + \frac{k^2}{8\pi} \int_{L_1}^{L} dx \left[\int_{-\infty}^{-2h_s(1 - x/L)} d\xi\, \frac{\sin\left(\frac{\xi kL(\xi/2 - m_1)}{x(L-x)} \right)}{\xi} \times b_{\mathrm{eff}}(0, \xi + 2h_s(1 - x/L)) - \int_{-2h_s(1 - x/L)}^{\infty} d\xi\, \frac{\sin\left(\frac{\xi kL(\xi/2 - m_2)}{x(L-x)} \right)}{\xi} b_{\mathrm{eff}}(0, \xi + 2h_s(1 - x/L)) \right], \quad (21)$$

$$\langle \chi_s^2 \rangle + \langle S_s^2 \rangle = \frac{k^2 L b_{\text{eff}}(0,0)}{8} + \frac{k^2}{4\pi} \int_0^L dx \int_0^\infty d\xi\, b_{\text{eff}}(0,\xi) \times \frac{\sin\left(\dfrac{\xi k L(-\xi/2 - m_1)}{x(L-x)} \right)}{\xi}, \tag{22}$$

$$\langle \chi_1^2 \rangle + \langle S_1^2 \rangle = \frac{k^2 L_1 b_{\text{eff}}(0,0)}{8} + \frac{k^2}{4\pi} \int_0^{L_1} dx \times \int_0^\infty d\xi\, b_{\text{eff}}(0,\xi) \frac{\sin\left(\dfrac{\xi k L(-\xi/2 - m_2)}{x(L-x)} \right)}{\xi}, \tag{23}$$

$$\langle \chi_2^2 \rangle + \langle S_2^2 \rangle = \frac{k^2 (L - L_1) b_{\text{eff}}(0,0)}{8} + \frac{k^2}{4\pi} \int_{L_1}^L dx \times \int_0^\infty d\xi\, b_{\text{eff}}(0,\xi) \frac{\sin\left(\dfrac{\xi k L(m_2 - \xi/2)}{x(L-x)} \right)}{\xi}. \tag{24}$$

In these equations,

$$m_1(x) = -(1 - x/L) h_s - x h_r / L, \quad m_2(x) = -(1 - x/L) h_s + x h_r / L, \tag{25}$$

and the function $b_{\text{eff}}(\mathbf{r})$ is given by[4]

$$b_{\text{eff}}(\mathbf{r}) = \int_{-\infty}^{\infty} B_{\text{eff}}(x, \mathbf{r}) dx = 2\pi \int d^2 K_\perp\, e^{i \mathbf{K}_\perp \cdot \mathbf{r}} \Phi_{\text{eff}}(0, \mathbf{K}_\perp). \tag{26}$$

Here, $B_{\text{eff}}(\mathbf{R})$ is the correlation function of the random field ϵ_{mov}, $\Phi_{\text{eff}}(\mathbf{K})$ is the three-dimensional spectral density of ϵ_{mov} and is related to B_{eff} by the Fourier transform: $B_{\text{eff}}(\mathbf{R}) = \int d^3 K e^{i \mathbf{K} \cdot \mathbf{R}} \Phi_{\text{eff}}(\mathbf{K})$, where $\mathbf{K} = (K_x, \mathbf{K}_\perp)$ is the wave vector, and $\mathbf{K}_\perp = (K_y, K_z)$. When deriving Eqs. (20)–(24), we used the Markov approximation: $B_{\text{eff}}(x, \mathbf{r}) = \delta(x) b_{\text{eff}}(\mathbf{r})$.

The correlation function B_{eff} can be expressed in terms of the correlation functions B_T and B_{xx} of the random fields $\tilde{T}$ and v_x, and the spectral density Φ_{eff} can be expressed in terms of the spectral densities Φ_T and Φ_{xx} of these random fields:[4]

$$B_{\text{eff}}(\mathbf{R}) = \frac{B_T(\mathbf{R})}{T_0^2} + \frac{4 B_{xx}(\mathbf{R})}{c_0^2}, \quad \Phi_{\text{eff}}(\mathbf{K}) = \frac{\Phi_T(\mathbf{K})}{T_0^2} + \frac{4 \Phi_{xx}(\mathbf{K})}{c_0^2}. \tag{27}$$

The term $\langle \chi_s S_i \rangle - \langle \chi_i S_s \rangle$ in the argument of cosine in Eq. (10) can be calculated analogously to the terms on the left-hand sides in Eqs. (20)–(24). It can be shown that the former term is much less than 1, and hence can be ignored. The same result is obtained in Refs. 1, 13.

Equations (20)–(24) can be simplified further. Let us consider the order of magnitudes of different terms in the argument of the sine in Eq. (22). First, the integration variable x satisfies the following relationship: $x(L-x) \sim L^2$. Second, since ξ is an argument of the function $b_{\text{eff}}(0,\xi)$ in the integrand in Eq. (22), it is of the order of the scale l of random inhomogeneities. Third, it follows from Eq. (25) that the function $m_1(x) \sim -h_m$, where h_m is a maximum of source and receiver heights [i.e., $h_m = \max(h_s, h_r)$]. Therefore, taking into account that $h_m \gg l$, we have $-\xi/2 - m_1 \sim h_m$. These estimates allow us to obtain the following relationship for the ratio of the sine and ξ in Eq. (22), which is denoted by s:

$$s = \frac{\sin\left(\dfrac{\xi k L(-\xi/2 - m_1)}{x(L-x)} \right)}{\xi} \sim \frac{\sin\left(\dfrac{\xi k h_m}{L} \right)}{\xi} = \frac{\sin\left(\dfrac{\xi}{l} \dfrac{h_m}{lD} \right)}{\xi}. \tag{28}$$

We assume that $D \ll h_m / l$. Since $D = L/(kl^2)$, this inequality is fulfilled for a relatively small distance L of sound propagation and/or for relatively high sound frequency $f = k c_0/(2\pi)$. The inequality $D \ll h_m/l$ is always valid in the geometrical acoustics approximation. It is also valid beyond the limits of this approximation because $h_m \gg l$. Since $D \ll h_m/l$, the argument of the sine in Eq. (28) is much greater than 1, and s is approximately equal to $\pi \delta(\xi)$.[20] Substituting the value of s into Eq. (22) and calculating the integrals over ξ and x, it can be shown that the second term on the right-hand side of this equation is equal to the first one. Analogously, it can be shown that for the considered case $D \ll h_m/l$, the second terms on the right-hand sides of Eqs. (20), (21), (23), and (24) are equal to the first terms.

Thus, the statistical moments on the left-hand sides of Eqs. (20)–(24) are just twice the first terms on the right-hand sides of these equations. Substituting the values of these statistical moments into Eq. (19) yields

$$C = \exp\left\{ -\frac{k^2 L}{4} \left[b_{\text{eff}}(0,0) - \frac{1}{2h_r} \int_0^{2h_r L_1/L} dz\, b_{\text{eff}}(0,z) - \frac{1}{2h_s} \int_0^{2h_s(1 - L_1/L)} dz\, b_{\text{eff}}(0,z) \right] \right\}. \tag{29}$$

Equation (29) is a generalization of formula for C in Ref. 1 for the case of both temperature and velocity fluctuations, and for the case of anisotropic spectra of these fluctuations. Furthermore, it will be shown at the end of the next subsection that C is given by Eq. (29) for all values of D if the Rytov approximation is valid. On the other hand, in Ref. 1 C is given by Eq. (29) only for $D \ll 1$ and is given by a different formula if $D \geqslant 1$. This difference is due to the fact that ground reflection of scattered waves is ignored in Ref. 1 as it is indicated in Refs. 12, 13. In the rest of this paper, we will obtain results [except Eq. (40)] that were not considered in Ref. 1.

D. Analysis of the coherence factor *C*

Taking into account the value of $L_1 = L/(h_r/h_s + 1)$, it can be shown that in Eq. (29) the upper limits of integration are the same: $2h_r L_1/L = 2h_s(1 - L_1/L) = 2h_s h_r/(h_s + h_r) = h$. Here, these limits are denoted by h. In the geometry in Fig. 1 and in the approximation of near-grazing propagation,

h is a maximum separation between the direct ray from source to receiver and that reflected from the ground. The use of h allows us to simplify Eq. (29):

$$C=\exp\left\{-\frac{k^2L}{4h}\int_0^h[b_{\rm eff}(0,0)-b_{\rm eff}(0,z)]dz\right\}. \tag{30}$$

Substituting $b_{\rm eff}$ from the right-hand side of Eq. (26) into Eq. (30), one obtains an expression for C in terms of $\Phi_{\rm eff}$:

$$C=\exp\left\{-\frac{\pi k^2L}{2h}\int_0^h dz\int d^2K_\perp\,\Phi_{\rm eff}(0,\mathbf{K}_\perp)[1-e^{iK_zz}]\right\}. \tag{31}$$

Accounting for the fact that $\Phi_{\rm eff}(0,\mathbf{K}_\perp)$ is an even function and calculating the integral over z yields

$$C=\exp\left\{-\frac{\pi k^2L}{2}\int d^2K_\perp\,\Phi_{\rm eff}(0,\mathbf{K}_\perp)\left[1-\frac{\sin(K_zh)}{K_zh}\right]\right\}. \tag{32}$$

This formula for C coincides with Eqs. (14) and (15) from Ref. 13 obtained in that reference by a different approach.

We now show that Eq. (30) is closely related to the coherence function of a spherical sound wave for line-of-sight propagation. A formula for the coherence function of a spherical electromagnetic wave for line-of-sight propagation is well known, e.g., Ref. 18. An approach presented in Ref. 4 allows us to generalize this formula for the case of a spherical sound wave propagating in a turbulent atmosphere with temperature and velocity fluctuations:

$$\begin{aligned}\Gamma(\mathbf{r};\mathbf{r}_+)&=\langle p(x,\mathbf{r}')p^*(x,\mathbf{r}'')\rangle\\&=\frac{\exp(ik\mathbf{r}\cdot\mathbf{r}_+/L)}{L^2}\\&\quad\times\exp\left\{-\frac{k^2}{4}\int_0^L[b_{\rm eff}(0)-b_{\rm eff}(\mathbf{r}\xi/L)]d\xi\right\}.\end{aligned} \tag{33}$$

Here, $\mathbf{r}=\mathbf{r}'-\mathbf{r}''$, and $\mathbf{r}_+=(\mathbf{r}'+\mathbf{r}'')/2$. We denote by $\hat\Gamma$ a normalized coherence function: $\hat\Gamma(\mathbf{r})=\Gamma(\mathbf{r};\mathbf{r}_+)/\Gamma^{(0)}(\mathbf{r};\mathbf{r}_+)$, where $\Gamma^{(0)}$ is the coherence function in a medium without random inhomogeneities. It follows from Eq. (33) that $\hat\Gamma$ is given by the second exponent on the right-hand side of this equation and does not depend on $\mathbf{r}_+$. Let $\mathbf{r}=(0,h)$, i.e., the two points of observation $\mathbf{r}'$ and $\mathbf{r}''$ are located on a vertical line at a distance h. Then, a comparison of Eq. (30) and the second exponent in Eq. (33) reveals that

$$C=\hat\Gamma(0,h)\equiv\frac{\Gamma(0,h;\mathbf{r}_+)}{\Gamma^{(0)}(0,h;\mathbf{r}_+)}. \tag{34}$$

Thus, the coherence factor C is equal to the normalized coherence function of a spherical sound wave for line-of-sight propagation.

Equations (30)–(34) are valid for anisotropic turbulence. Let us now consider the case of isotropic turbulence. In this case, $\Phi_{\rm eff}(0,\mathbf{K}_\perp)$ is given by Ref. 4:

$$\Phi_{\rm eff}(0,\mathbf{K}_\perp)=\frac{\Phi_T(K_\perp)}{T_0^2}+\frac{4F(K_\perp)}{c_0^2}, \tag{35}$$

where $F(K_\perp)$ is the three-dimensional spectral density of velocity fluctuations related to Φ_{xx} by $\Phi_{xx}(\mathbf{K})=(1-K_x^2/K^2)F(K)$. Substituting Eq. (35) into Eq. (31) and calculating the integral over the azimuthal directions of the vector $\mathbf{K}_\perp$, one obtains

$$C=\exp\left\{-\pi^2k^2L\int_0^1dt\int_0^\infty\left[\frac{\Phi_T(K)}{T_0^2}+\frac{4F(K)}{c_0^2}\right]\times[1-J_0(hKt)]KdK\right\}, \tag{36}$$

where J_0 is the Bessel function of zero the order.

The relationship (34) holds for isotropic turbulence also. For such turbulence, the coherence function $\Gamma(\mathbf{r};\mathbf{r}_+)$ is presented in Ref. 4 for the Kolmogorov, Gaussian, and von Karman spectra of temperature and velocity fluctuations. These spectra have been most widely used in atmospheric acoustics. Equation (34) and formulas for $\Gamma(\mathbf{r};\mathbf{r}_+)$ from Ref. 4 allow us to calculate the coherence factor C for these spectra. For the Kolmogorov spectra of temperature and velocity fluctuations, $\Phi_T(K)$ and $F(K)$ are given by[3,4]

$$\Phi_T^{\rm K}(K)=AC_T^2K^{-11/3},\quad F^{\rm K}(K)=(11/6)AC_v^2K^{-11/3}. \tag{37}$$

Here, the superscript ''K'' refers to the Kolmogorov spectrum, $A\approx0.0330$, and C_T^2 and C_v^2 are the structure parameters of temperature and velocity fluctuations. The Kolmogorov spectrum is a realistic spectrum of isotropic turbulence in the inertial subrange (e.g., Sec. 6.2.3 in Ref. 4). It does not describe a spectrum of turbulence due to eddies larger than those in the inertial subrange. For the Kolmogorov spectrum, the coherence factor C can be found with the use of Eq. (34) and Eq. (7.83) for $\Gamma(\mathbf{r};\mathbf{r}_+)$ from Ref. 4:

$$C^K=\exp\left\{-k^2h^{5/3}L\frac{3BC_T^2}{8T_0^2}-k^2h^{5/3}L\frac{11BC_v^2}{4c_0^2}\right\}, \tag{38}$$

where the coefficient $B\approx0.364$.

For the Gaussian spectra of temperature and velocity fluctuations, $\Phi_T(K)$ and $F(K)$ are given by[4]

$$\Phi_T^{\rm G}(K)=\frac{\sigma_T^2l^3}{8\pi^{3/2}}e^{-K^2l^2/4},\quad F^{\rm G}(K)=\frac{\sigma_v^2K^2l^5}{32\pi^{3/2}}e^{-K^2l^2/4}, \tag{39}$$

where superscript ''G'' refers to the Gaussian spectrum, σ_T^2 and σ_v^2 are the variances of temperature and velocity fluctuations, and l is the scale of random inhomogeneities. For this spectrum, the coherence factor C can be obtained by making use of Eq. (34) and Eq. (7.107) for $\Gamma(\mathbf{r};\mathbf{r}_+)$ from Ref. 4:

$$\begin{aligned}C^{\rm G}=\exp\Bigg\{&-2\gamma_T^{\rm G}L\left[1-\frac{\sqrt{\pi}l}{2h}\,{\rm erf}\left(\frac{h}{l}\right)\right]\\&-2\gamma_v^{\rm G}L\left[1-\frac{\sqrt{\pi}l}{4h}\,{\rm erf}\left(\frac{h}{l}\right)-\frac{1}{2}e^{-h^2/l^2}\right]\Bigg\}.\end{aligned} \tag{40}$$

Here, $\gamma_T^{\rm G}=\sqrt{\pi}k^2\sigma_T^2l/(8T_0^2)$ is the extinction (attenuation) coefficient of the mean sound field due to temperature fluctuations with the Gaussian spectrum, $\gamma_v^{\rm G}=\sqrt{\pi}k^2\sigma_v^2l/(2c_0^2)$ is that due to velocity fluctuations, and erf(h/l) is the error func-

tion. If $\sigma_v^2=0$, Eq. (40) coincides with the corresponding equation in Ref. 1.

For the von Karman spectra of temperature and velocity fluctuations, $\Phi_T(K)$ and $F(K)$ are given by[4]

$$\Phi_T^{\mathrm{vK}}(K)=AC_T^2(K^2+K_0^2)^{-11/6},$$
$$F^{\mathrm{vK}}(K)=\tfrac{11}{6}AC_v^2K^2(K^2+K_0^2)^{-17/6}. \tag{41}$$

Here, the superscript ''vK'' refers to the von Karman spectrum, and K_0 is the wavenumber which is inversely proportional to the outer scale of turbulence. The coherence factor C can be obtained with the use of Eq. (34) and Eq. (7.114) for $\Gamma(\mathbf{r};\mathbf{r}_+)$ from Ref. 4:

$$C^{\mathrm{vK}}=\exp\left\{-\frac{2L}{K_0h}\int_0^{K_0h}dt\left[\gamma_T^{\mathrm{vK}}\left[1-\frac{2^{1/6}t^{5/6}}{\Gamma(5/6)}K_{5/6}(t)\right]\right.\right.$$
$$\left.\left.+\gamma_v^{\mathrm{vK}}\left[1-\frac{2^{1/6}t^{5/6}}{\Gamma(5/6)}\left(K_{5/6}(t)-\frac{t}{2}K_{1/6}(t)\right)\right]\right]\right\}. \tag{42}$$

Here, $K_\nu(t)$ is the modified Bessel function, $\gamma_T^{\mathrm{vK}}=3\pi^2Ak^2K_0^{-5/3}C_T^2/(10T_0^2)$ is the extinction coefficient of the mean sound field due to temperature fluctuations with the von Karman spectrum, and $\gamma_v^{\mathrm{vK}}=6\pi^2Ak^2K_0^{-5/3}C_v^2/(5c_0^2)$ is that due to velocity fluctuations.

At the end of this section, let us consider the range of applicability of Eqs. (30)–(32) and (36). These equations have been derived for the case of geometrical acoustics ($D\ll1$), and for the case of Fraunhofer diffraction ($D\gg1$) if

$$h_0>\sqrt{L/k},\quad D\ll h_m/l. \tag{43}$$

Two facts indicate that Eqs. (30)–(32) and (36) are valid even if inequalities (43) are not fulfilled. First, the results obtained in Ref. 13 show that the range of applicability of Eq. (32) does not require validity of these inequalities. Second, Ref. 21 considers the interference of the direct and ground-reflected electromagnetic waves in an atmosphere with fluctuations ϵ in the dielectric permittivity. The geometry of the problem in Ref. 21 is similar to that in Fig. 1. Starting from the parabolic equation for the electromagnetic field E, using the Feynman path-integral technique, and assuming that the ground is perfectly reflecting ($Q=-1$), the following formula for the mean squared field $\langle|E|^2\rangle$ is obtained in Ref. 21:

$$\langle|E|^2\rangle=\frac{2}{L^2}\left[1-\exp\left(-\frac{\pi k^2L}{4}\int_0^1d\xi\,H(h\xi)\right)\right.$$
$$\left.\times\cos(2kh_sh_r/L)\right], \tag{44}$$

where

$$H(\mathbf{r})=2\int d^2K_\perp\Phi_\epsilon(0,\mathbf{K}_\perp)[1-e^{i\mathbf{K}_\perp\cdot\mathbf{r}}]. \tag{45}$$

Here, $\Phi_\epsilon(K_x,\mathbf{K}_\perp)$ is the three-dimensional spectral density of ϵ. The range of applicability of Eqs. (44) and (45) is that of the Rytov method. Note that inequalities (43) have not been used when deriving Eqs. (44) and (45).

According to Ref. 4, Eqs. (44) and (45) can be used to obtain a formula for $\langle|p|^2\rangle$ for the case of sound propagation near the ground in the atmosphere with temperature and velocity fluctuations. The formula for $\langle|p|^2\rangle$ is given by the right-hand side of Eq. (44) if $\Phi_\epsilon(0,\mathbf{K}_\perp)$ is replaced by $\Phi_{\mathrm{eff}}(0,\mathbf{K}_\perp)$. This formula coincides with Eq. (10), where C is given by Eq. (36) if in Eq. (10) $|Q|=1$, $\Omega=\pi$, $\langle\chi_sS_i\rangle-\langle\chi_iS_s\rangle=0$, $R_s=R_i=L$, and $R_i-R_s=2h_sh_r/L$. The latter two equalities are always valid in the approximation of near-grazing propagation. Therefore, if $Q=-1$, Eqs. (44) and (45) derived in Ref. 21 lead to the same formula for $\langle|p|^2\rangle$ that is obtained in the present paper.

Thus, we can conclude that the range of applicability of Eqs. (30)–(32) and (36) is not limited by inequalities (43), and is the same as the range of applicability of the Rytov method, which is known in the literature (e.g., Ref. 17). The latter range includes a condition that amplitude fluctuations in the direct wave are not saturated (i.e., $\langle\chi_s^2\rangle\ll1$).

IV. NUMERICAL AND EXPERIMENTAL RESULTS

A. Isotropic turbulence

In this and next subsections, Eqs. (10), (38), (40), and (42) are used to numerically study the effects of atmospheric turbulence on the relative sound pressure level W, which is related to $\langle|p|^2\rangle$ by

$$W=10\log(\langle|p|^2\rangle/p_0^2), \tag{46}$$

where $p_0=1/r_0$ is the amplitude of the sound pressure due to the source at a distance $r_0=1$ m.

In the numerical examples below, the source and receiver heights above the ground are $h_s=6$ m and $h_r=3$ m, respectively; the horizontal distance between them is $L=130$ m; the adiabatic sound speed $c_0=340$ m/s; and the ground is acoustically hard, i.e., $|Q|=1$ and $\Omega=0$. We denote by W_0 the relative sound pressure level in the atmosphere without turbulence. Here W_0 is given by Eqs. (46) and (10) with $C=1$. Figure 3 shows the dependence of W_0 on the sound frequency f. The interference of the direct and ground-reflected waves results in maxima and minima in the dependence of W_0 on f.

The solid line in Fig. 4 reproduces the first minimum of W_0 in a more narrow frequency range from 595 to 635 Hz. The dotted, dash–dotted, and dashed lines correspond to the relative sound pressure levels W_v^{K}, W_v^{G}, and W_v^{vK} in a turbulent atmosphere having velocity fluctuations only ($\tilde{T}=0$), with the Kolmogorov, Gaussian, and von Karman spectra, respectively. Here W_v^{K}, W_v^{G}, and W_v^{vK} are given by Eqs. (46) and (10), where C is given by Eqs. (38), (40), and (42), respectively. In Fig. 4, $l=1$ m and $C_v^2=8\times10^{-8}c_0^2\,\mathrm{m}^{-2/3}$. Furthermore, the values of K_0 and σ_v^2 are chosen from the following relationships:

$$K_0=\frac{2\Gamma(5/6)}{\Gamma(1/3)l},\quad \sigma_v^2=\frac{\Gamma^2(1/3)}{\pi2^{4/3}\sqrt{3}}C_v^2K_0^{-2/3}, \tag{47}$$

where Γ is the gamma-function. These relationships between the parameters of the Gaussian and von Karman spectra of velocity fluctuations are used to compare the statistical moments of a sound field for these spectra, see Eqs. (6.49) and (6.51) from Ref. 4. If the relationships (47) are valid, the

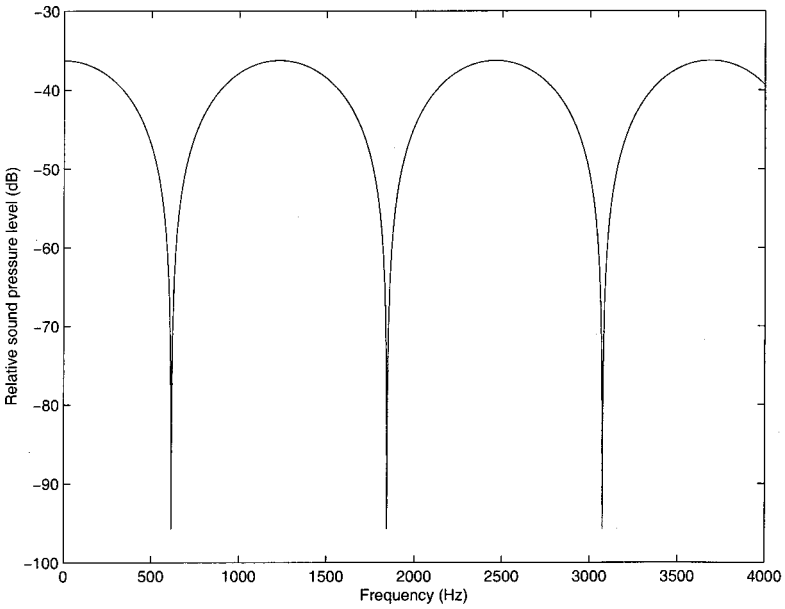

FIG. 3. Relative sound pressure level W_0 versus the frequency f in the atmosphere without turbulence.

integral lengths of the von Karman and Gaussian spectra of velocity fluctuations are equal, and the variances of these spectra are the same. Furthermore, $\gamma_v^{\mathrm{vK}}=\gamma_v^{\mathrm{G}}$ if Eq. (47) is valid.

It follows from Fig. 4 that the relative sound pressure levels for the Gaussian and von Karman spectra, W_v^{G} and W_v^{vK}, are very close to each other. On the other hand, the relative sound pressure level for the Kolmogorov spectrum, W_v^{K}, significantly differs from W_v^{G} and W_v^{vK}. This can be explained by using results obtained in Ref. 22. It follows from this reference that, if $\gamma_v^{\mathrm{vK}}L=\gamma_v^{\mathrm{G}}L<0.5$, the coherence function Γ_v^{vK} of a spherical sound wave for line-of-sight propagation in the atmosphere having velocity fluctuations with the von Karman spectrum nearly coincides with the coherence function Γ_v^{G} for the case of Gaussian spectrum and significantly differs from the coherence function Γ_v^{K} for the Kolmogorov spectrum. On the other hand, if $\gamma_v^{\mathrm{vK}}L=\gamma_v^{\mathrm{G}}L$ is greater than 100, Γ_v^{vK} nearly coincides with Γ_v^{K} and significantly differs from Γ_v^{G}. For the values of the parameters in Fig. 4, $\gamma_v^{\mathrm{vK}}L=\gamma_v^{\mathrm{G}}L\sim 7\times 10^{-4}$. Therefore, in this case $\Gamma_v^{\mathrm{vK}}\sim\Gamma_v^{\mathrm{G}}$, and Γ_v^{vK} significantly differs from Γ_v^{K}. Since the coherence factor C and the coherence function Γ are related by Eq. (34), one can conclude that $W_v^{\mathrm{vK}}\sim W_v^{\mathrm{G}}$, and that W_v^{vK} significantly differs from W_v^{K}. This explains Fig. 4.

Considerations above allow us also to conclude that, if $\gamma_v^{\mathrm{vK}}L=\gamma_v^{\mathrm{G}}L>100$, the coherence factor C for the von Karman spectrum is nearly the same as that for the Kolmogorov spectrum, and differs significantly from C for the Gaussian spectrum. However, in this case the coherence factors C for these spectra are much less than 1 since γ_v^{G} and γ_v^{vK} are in the exponents in Eqs. (40) and (42). Therefore, $W_v^{\mathrm{K}}\approx W_v^{\mathrm{G}}\approx W_v^{\mathrm{vK}}$ because the third term (which is proportional to C) on the right-hand side of Eq. (10) can be ignored.

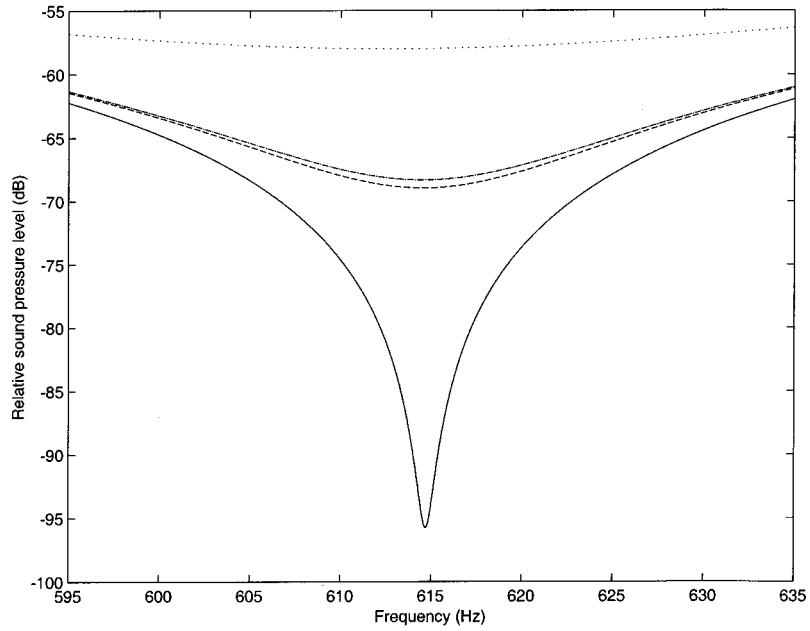

FIG. 4. Relative sound pressure level versus the frequency f. Solid, dashed, dash–dotted, and dotted lines correspond to the cases of atmosphere without turbulence, and with von Karman, Gaussian, and Kolmogorov spectra of velocity fluctuations.

Let us now study the effects of temperature and velocity contributions to the relative sound pressure levels W^{K}, W^{G}, and W^{vK} for the Kolmogorov, Gaussian, and von Karman spectra. Equations (38), (40), and (42) clearly show that these contributions to the coherence factor C and, hence, to W are different. Numerical calculations show that the maximum difference between the sound pressure levels W^{K}, W^{G}, and W^{vK} in the atmosphere with temperature fluctuations only and those in the atmosphere with velocity fluctuations only is a few dB. When comparing temperature and velocity contributions to W^{K}, W^{G}, and W^{vK}, we assumed that $C_T^2/T_0^2 = 4C_v^2/c_0^2$. This relationship is employed to compare the relative contributions from temperature and velocity fluctuations to the statistical moments of a sound field (e.g., Ref. 4). If this relationship were valid, the temperature and velocity contributions to the structure parameter of acoustic refractive index fluctuations would be the same.

B. Anisotropic turbulence

Now let us consider the effects of turbulent anisotropy on the interference of the direct and ground-reflected waves. For anisotropic turbulence, it is convenient to express the velocity component along the x-axis in the following form: $v_x(\mathbf{R}) = v_1(\mathbf{R})\cos\theta + v_2(\mathbf{R})\sin\theta$. Here v_1 is the component of $\mathbf{v}(\mathbf{R})$ in the direction of the mean wind, v_2 is the component crosswind, and θ is the angle between the horizontal component of the mean wind velocity vector and the x-axis. In this case, ϵ_{mov} is reexpressed as $\epsilon_{\mathrm{mov}} = -\tilde{T}/T_0 - 2(v_1\cos\theta + v_2\sin\theta)/c_0$. Using this formula, the following expression for $\Phi_{\mathrm{eff}}(\mathbf{K})$ can be obtained:

$$\Phi_{\mathrm{eff}}(\mathbf{K}) = \frac{\Phi_T(\mathbf{K})}{T_0^2} + \frac{4}{c_0^2}[\Phi_{11}(\mathbf{K})\cos^2\theta + \Phi_{12}(\mathbf{K})\sin(2\theta) + \Phi_{22}(\mathbf{K})\sin^2\theta], \tag{48}$$

and likewise for the correlation function $B_{\mathrm{eff}}(\mathbf{R})$. In Eq. (48), Φ_{11}, Φ_{12}, and Φ_{22} are the three-dimensional spectral densities of the correlation functions $\langle v_1(\mathbf{R})v_1(\mathbf{R}')\rangle$, $\langle v_1(\mathbf{R})v_2(\mathbf{R}')\rangle$, and $\langle v_2(\mathbf{R})v_2(\mathbf{R}')\rangle$, respectively.

We will use Mann's anisotropic rapid-distortion model[23] for the turbulent velocity field. This model was derived from an isotropic von Karman spectrum by calculating distortions to the turbulence resulting from a constant vertical wind shear. Since the spectral equations for Mann's model are rather complicated and have been given elsewhere,[7,23] they will not be repeated here. The geometry of the problem is the same as in Figs. 3 and 4. The application of Mann's model in this paper is the same as in Wilson:[7] the dimensionless shear parameter, Γ (not to be confused with the coherence function), is set to 3.58; the variance parameter is $\sigma_M^2 = 1.52u_*^2$ (where u_* is the friction velocity); and the length scale is $l_M = 0.587z$. Because the length scale in Mann's model is height-dependent, we are forced to assign z to a representative value in order to calculate the length scale. Therefore we somewhat arbitrarily set $z = 4$ m, resulting in $l_M = 2.35$ m. The friction velocity can be determined from the velocity variance. Based on Eq. (47), the variance for our example is $\sigma_v^2 = 0.00542\ \mathrm{m}^2/\mathrm{s}^2$. Taking $\sigma_v^2 = 2.97u_*^2$ in the isotropic von Karman model,[7] one has $u_* = 0.0427$ m/s. (The variance σ_v^2 and friction velocity u_* in this example are characteristic of very low wind atmospheric conditions.)

Calculations for along mean wind and crosswind propagation using the Mann model are shown in Fig. 5. Also shown for comparison is the isotropic von Karman model, with $\sigma_v^2 = 2.97u_*^2$ and $K_0^{-1} = 1.79z = 7.16$ m,[7] where K_0 is a parameter in Eq. (41). The effect of the turbulence on filling in the interference minimum is about 4 dB larger in the along-wind than in the crosswind direction. The prediction for the isotropic von Karman model falls in between. This behavior results from the higher variance and extended integral length scale in the along-wind direction characteristic of a shear layer.

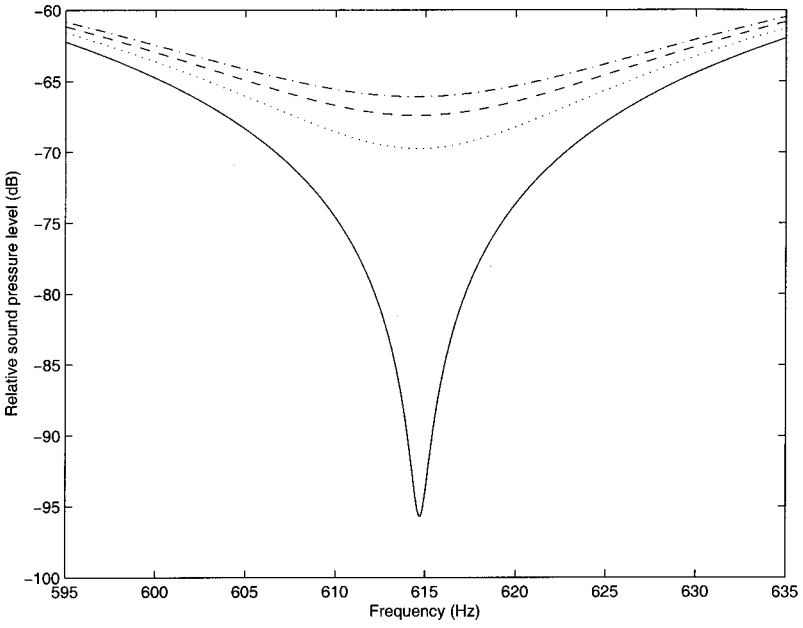

FIG. 5. Relative sound pressure level versus the frequency f. Solid, dashed, dash–dotted, and dotted lines correspond to the cases of the atmosphere without turbulence, and isotropic von Karman, Mann along-wind, and Mann crosswind spectra of velocity fluctuations.

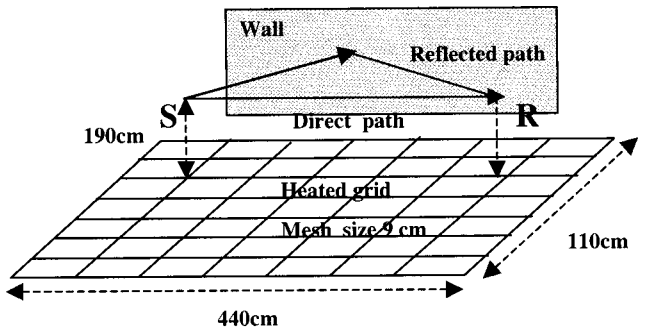

FIG. 6. The geometry of the laboratory experiment. S is a point monochromatic source, and R is a receiver (microphone).

C. Comparison between theory and experiment

Here, we compare mean squared sound pressure $\langle|p|^2\rangle$ calculated for the von Karman spectrum of temperature fluctuations [see Eqs. (10) and (42)] with experimental data obtained in a large anechoic chamber in Ecole Centrale de Lyon.[24]

In the experiment, temperature fluctuations were created by a heated grid located horizontally (see Fig. 6). The size of the grid was 440×110 cm and the size of a mesh in the grid was 9 cm. A spectrum of temperature fluctuations above the grid is approximated very well by the von Karman spectrum $\Phi_T^{\mathrm{vK}}(K)$ given by Eq. (41). The parameters K_0 and C_T^2 of this spectrum, measured in the experiment, were as follows: $K_0=6.8\,\mathrm{m}^{-1}$ and $C_T^2/T_0^2=3.36\times10^{-4}\,\mathrm{m}^{-2/3}$. The value of C_T^2 is normalized by T_0^2 since γ_T^{vK} in Eq. (42) for the coherence factor C^{vK} is proportional to C_T^2/T_0^2.

An acoustically hard wall was vertically placed above the grid. A point monochromatic source and a microphone were also placed above the grid at the distances h_s and h_r from the wall. For this geometry, two waves are impinging on the receiver: the direct wave and that reflected from the wall. In the experiment, time-mean squared pressure $\langle|p|^2\rangle$ was measured as a function of the distance L between the source and microphone. The distance h_s was 10 cm; L varied from 3 cm to 3 m; and the measurements were done for $h_r=7$ and 10 cm, and $f=23.5$, 31, 40, and 75 kHz. For this geometry, the values of the wave parameter D and the variances of log-amplitude and phase fluctuations $\langle\chi_s^2\rangle$ and $\langle S_s^2\rangle$ are close to those for sound propagation in the atmosphere. Furthermore, the relationship $L\gg K_0^{-1}\gg k^{-1}$ between parameters of the experiment usually holds for outdoor sound propagation also. Therefore, the laboratory experiment in question models sound propagation in a turbulent atmosphere.

In the experiment, a reference microphone was located at a distance 2 cm from the source. Using the measured values of $\langle|p|^2\rangle$ and the pressure p_0 at the reference microphone, the relative sound pressure level W was calculated with the use of Eq. (46). Then, the dependence of W versus L was plotted for fixed values of h_r and f. One of these dependences, obtained for $h_r=7$ cm and $f=40$ kHz, is shown in Fig. 7 by the ''+'' symbol. Interference maxima and minima are clearly seen in the figure as well as a decrease of W with an increase of L due to spherical spreading.

In Fig. 7, the solid line is the theoretical predictions of the relative sound pressure level W for the von Karman spectrum of temperature fluctuations. W was calculated with the use of Eqs. (10), (42), and (46), where the values of parameters were taken from the experiment: $Q=1$, $f=40$ kHz, $h_s=10$ cm, $h_r=7$ cm, $K_0=6.8\,\mathrm{m}^{-1}$, and $C_T^2/T_0^2=3.36\times10^{-4}\,\mathrm{m}^{-2/3}$. Figure 7 shows good agreement between theoretical predictions and experimental data.

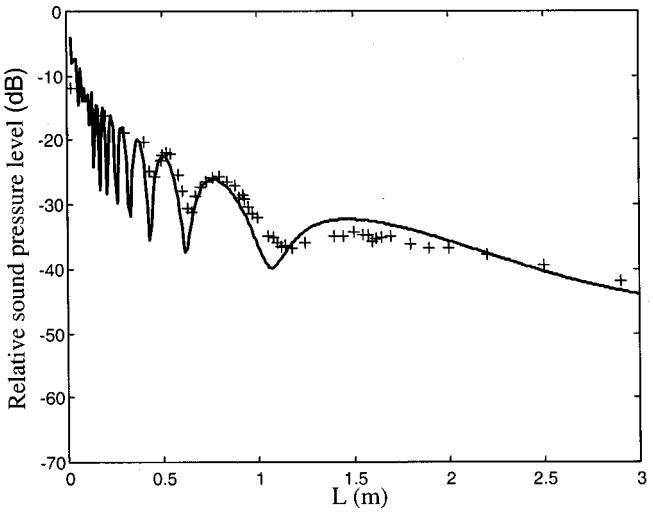

FIG. 7. Relative sound pressure level W versus the distance L between the source and the receiver for $f=40$ kHz, $h_s=10$ cm, and $h_r=7$ cm. The solid line corresponds to theoretical predictions; symbols ''+'' correspond to experimental data obtained in the laboratory experiment.

For other values of h_r and f, theoretical predictions and experimental data also agree well. A more detailed description of the experimental setup and comparison between data and theoretical predictions is present in Refs. 6 and 25.

V. CONCLUSIONS

We have studied sound propagation near the impedance ground in the atmosphere with temperature and velocity fluctuations when a sound field p is the sum of the direct and ground-reflected waves; see Fig. 1. We have shown that, when calculating p, the geometry of Fig. 1 can be replaced by a new geometry shown in Fig. 2. In this new geometry, the ground is removed, a random medium fills the whole space, and the source is supplemented by an image source. The sound field p at the receiver is the sum of the sound field emitted by the source, and that emitted by the image source. We gave a mathematical formulation of the geometry in Fig. 2, which is based on the parabolic equation (3) for p, initial condition (5), and Eq. (4) which determines the random inhomogeneities in a medium. Equations (3), (4), and (5) for calculating p are the first important result obtained in the paper.

We used the Rytov method to solve the parabolic equation (3) and obtained expressions for the complex phases ψ_s and ψ_i of the waves emitted by the source and the image source. We also derived Eq. (10) for the mean squared sound pressure $\langle|p|^2\rangle$. This equation contains the coherence factor C which characterizes the coherence between the waves emitted by the source and the image source. Using expressions for ψ_s and ψ_i, we obtained Eq. (29) for C. Equations

(10) and (29) for $\langle|p|^2\rangle$ and C, respectively, generalize those obtained by Clifford and Lataitis[1] for the case of both temperature and velocity fluctuations, and for the case of anisotropic spectra of these fluctuations. Furthermore, we have shown that C is given by Eq. (29) for all values of the wave parameter D if the Rytov approximation is valid. This generalization is the second important result of the present paper.

Then, we showed that the coherence factor C is equal to the normalized coherence function $\hat{\Gamma}$ of a spherical sound wave for line-of-sight propagation. For the case of isotropic turbulence, the coherence function has been recently calculated for the Kolmogorov, Gaussian, and von Karman spectra of temperature and velocity fluctuations.[4] This allowed us to obtain analytical expressions (38), (40), and (42) for C for these spectra. This is the third important result of the paper.

Using the obtained expressions for C, we numerically compared the relative sound pressure levels W for the Kolmogorov, Gaussian, and von Karman spectra of velocity fluctuations. Then, we numerically studied the relative contributions from temperature and velocity fluctuations to W for the Kolmogorov, Gaussian, and von Karman spectra of these fluctuations. Also, the effects of turbulent anisotropy on the interference of direct and ground-reflected waves was numerically studied. Finally, we showed that the theoretical predictions of the relative sound pressure level for the von Karman spectrum of temperature fluctuations are in a good agreement with experimental data obtained in a laboratory experiment.

ACKNOWLEDGMENTS

This material is partly based upon work that was supported by the U.S. Army Research Office under Contract No. DAAG55-98-1-0463, and NRC-ETL Research Associateship.

APPENDIX A: EQUIVALENCE OF GEOMETRIES IN FIGS. 1 AND 2

In this appendix, we show the equivalence of the geometries in Figs. 1 and 2 for the case $Q=1$. In the analysis below, we assume that a source is located at the point $\mathbf{R}_0=(x_0,y_0,z_0)$ which may not coincide with the origin of the coordinate system. The receiver is located at the point $\mathbf{R}=(x,y,z)$.

Let us derive an integral equation for the sound pressure $p(\mathbf{R},\mathbf{R}_0)$ due to the point source for the geometry in Fig. 1. If there are no random inhomogeneities in the atmosphere, $p(\mathbf{R},\mathbf{R}_0)$ is equal to the Green's function $G(\mathbf{R},\mathbf{R}_0)$ of the problem, given by

$$G(\mathbf{R},\mathbf{R}_0)=G_0(\mathbf{R}-\mathbf{R}_0)+Q(\mathbf{R},\mathbf{R}_0)G_0(\mathbf{R}-\mathbf{R}_0'). \tag{A1}$$

Here, $G_0(\mathbf{R})=R^{-1}e^{ikR}$ is the Green's function in a free space, and $\mathbf{R}_0'=(x_0,y_0,-z_0-2h_s)$ is a point symmetrical to $\mathbf{R}_0=(x_0,y_0,z_0)$ with respect to the ground surface $z=-h_s$. In Eq. (A1), we take into account that Q depends on the positions of the source and the receiver. Equation (A1) is a generalization of Eq. (1) for the case of arbitrary positions of the source and the receiver.

If there are fluctuations in the acoustic refractive index in the atmosphere, given by $\epsilon_{\mathrm{mov}}/2$, the sound field $p(\mathbf{R},\mathbf{R}_0)$ satisfies the following integral equation:

$$p(\mathbf{R},\mathbf{R}_0)=G(\mathbf{R},\mathbf{R}_0)+k^2\int_{-\infty}^{\infty}dx_1\int_{-\infty}^{\infty}dy_1 \times\int_{-h_s}^{\infty}dz_1\,\epsilon_{\mathrm{mov}}(\mathbf{R}_1)G(\mathbf{R},\mathbf{R}_1)p(\mathbf{R}_1,\mathbf{R}_0). \tag{A2}$$

To show that Eq. (A2) correctly describes sound propagation in the turbulent atmosphere near the impedance ground, one can solve this equation by iterations, replacing $p(\mathbf{R}_1,\mathbf{R}_0)$ in the integrand by the right-hand side of this equation. The resulting Born series describes a process of multiple scattering of p in a turbulent atmosphere near the ground.

For the geometry in Fig. 2, an integral equation for the sound pressure $p(\mathbf{R},\mathbf{R}_0)$ can be derived analogously to the derivation of Eq. (A2):

$$p(\mathbf{R},\mathbf{R}_0)=G(\mathbf{R},\mathbf{R}_0)+k^2\int_{-\infty}^{\infty}dx_1\int_{-\infty}^{\infty}dy_1 \times\int_{-\infty}^{\infty}dz_1\,\mu(\mathbf{R}_1)G_0(\mathbf{R}-\mathbf{R}_1)p(\mathbf{R}_1,\mathbf{R}_0). \tag{A3}$$

We point out some similarities and differences between Eqs. (A2) and (A3). If $\epsilon_{\mathrm{mov}}=0$, it follows from Eq. (A3) that $p=G(\mathbf{R},\mathbf{R}_0)$, as it should. Since there is no boundary for the geometry in Fig. 2, the Green's function is equal to $G_0(\mathbf{R}-\mathbf{R}_1)$ rather than to $G(\mathbf{R},\mathbf{R}_0)$; G_0 is in the integrand in Eq. (A3). The integration over z_1 in Eq. (A3) is from $-\infty$ to ∞, while that in Eq. (A2) is from $-h_s$ to ∞.

We now show that Eqs. (A2) and (A3) are equivalent. We denote by I_z the integral over z_1 in Eq. (A3):

$$I_z=\int_{-\infty}^{\infty}dz_1\,\mu(\mathbf{R}_1)G_0(\mathbf{R}-\mathbf{R}_1)p(\mathbf{R}_1,\mathbf{R}_0). \tag{A4}$$

We split this integral into two: the first from $-h_s$ to ∞, the second from $-\infty$ to $-h_s$. In the latter integral, we change the integration variable from z_1 to $z_2=-z_1-h_s$. The limits of integration over z_2 are from $-h_s$ to ∞. Then, denoting $z_2=z_1$, one obtains

$$I_z=\int_{-h_s}^{\infty}dz_1[\mu_{\mathrm{mov}}(\mathbf{R}_1)G_0(\mathbf{R}-\mathbf{R}_1)p(\mathbf{R}_1,\mathbf{R}_0) +\mu_{\mathrm{mov}}(\mathbf{R}_1')G_0(\mathbf{R}-\mathbf{R}_1')p(\mathbf{R}_1',\mathbf{R}_0)], \tag{A5}$$

where $\mathbf{R}_1'=(x_1,y_1,-z_1-2h_s)$ is a point symmetrical to $\mathbf{R}_1=(x_1,y_1,z_1)$ with respect to the plane $z=-h_s$.

It can be shown that $p(\mathbf{R},\mathbf{R}_0)=p(\mathbf{R}',\mathbf{R}_0)$, where $\mathbf{R}'=(x,y,-z-2h_s)$ is a point of the image receiver (see Fig. 2), and $p(\mathbf{R}',\mathbf{R}_0)$ is the sound pressure at this point. Indeed, $p(\mathbf{R},\mathbf{R}_0)$ is the sum of the sound fields of two waves propagating along the line segments OR and $O'R$, while $p(\mathbf{R}',\mathbf{R}_0)$ is the sum of the sound fields of the waves propagating along $O'R'$ and OR'. Taking into account that μ is symmetrical with respect to the plane $z=-h_s$, it is clear that

the line segments OR and $O'R'$ pass through the same inhomogeneities; so do $O'R$ and OR'. This proves that $p(\mathbf{R},\mathbf{R}_0)=p(\mathbf{R}',\mathbf{R}_0)$. Therefore, in Eq. (A5), $p(\mathbf{R}_1,\mathbf{R}_0)=p(\mathbf{R}_1',\mathbf{R}_0)$. Furthermore, using Eq. (4), it is easy to show that in Eq. (A5), $\mu(\mathbf{R}_1)=\mu(\mathbf{R}_1')=\epsilon_{\mathrm{mov}}(\mathbf{R}_1)$.

Using these equalities in Eq. (A5) for I_z and substituting the value of I_z into Eq. (A3) yields

$$p(\mathbf{R},\mathbf{R}_0)=G(\mathbf{R},\mathbf{R}_0)+k^2\int_{-\infty}^{\infty}dx_1\int_{-\infty}^{\infty}dy_1 \times\int_{-h_s}^{\infty}dz_1\,\epsilon_{\mathrm{mov}}(\mathbf{R}_1)p(\mathbf{R}_1,\mathbf{R}_0) \times[G_0(\mathbf{R}-\mathbf{R}_1)+G_0(\mathbf{R}-\mathbf{R}_1')]. \tag{A6}$$

This equation is equivalent to Eq. (A2) if $Q=1$ and differs from it if $Q\neq 1$.

In the geometry of Fig. 2, $p(\mathbf{R},\mathbf{R}_0)$ is the sum of the sound fields propagating along the line segments OR and $O'R$. The latter line segment passes through the same inhomogeneities as the line segment OR' from the source to the image receiver. Therefore, one can conclude that $p(\mathbf{R},\mathbf{R}_0)$ is equal to the sound fields along the line segments OR and OR'. In other words, $p(\mathbf{R},\mathbf{R}_0)$ can be represented as the sum of the sound fields at the receiver and image receiver, which are emitted by the source. This result is used in Ref. 13.

APPENDIX B: CALCULATION OF THE COHERENCE FACTOR *C*

In Appendix B, expressions for $\overline{\chi_s}$, $\overline{\chi_i}$, $\overline{S_s}$, and $\overline{S_i}$ are obtained, which are then used in deriving a formula for the coherence factor C.

The random fields $\psi_s=\chi_s+iS_s$ and $\psi_i=\chi_i+iS_i$ have Gaussian destributions. We remind the reader of a well-known formula (e.g., Refs. 1, 17):

$$\langle\exp(\xi)\rangle=\exp(\tfrac{1}{2}\langle(\xi-\overline{\xi})^2\rangle+\overline{\xi}), \tag{B1}$$

which is valid for a random field ξ having a Gaussian distribution. This formula allows one to express the mean value of e^{ξ} in terms of the mean value and variance of the random field ξ.

The equality $\langle e^{\psi_s+\psi_s^*}\rangle=1$, which is used to derive Eq. (10), can also be written as $\langle e^{2\chi_s}\rangle=1$. Using Eq. (B1), the latter equality can be rewritten in the following form:

$$\exp(2\langle\chi_s^2\rangle-2(\overline{\chi_s})^2+2\overline{\chi_s})=1. \tag{B2}$$

This equation is equivalent to the following equation: $\langle\chi_s^2\rangle-(\overline{\chi_s})^2+\overline{\chi_s}=0$. It follows from the latter equation that

$$\overline{\chi_s}=-\langle\chi_s^2\rangle+O(\langle\epsilon_{\mathrm{mov}}^4\rangle). \tag{B3}$$

Let us now derive a formula for the mean value of phase fluctuations $\overline{S_s}$. Consider the mean sound field of the wave emitted by the source:

$$\langle p_s\rangle=\frac{e^{ikR_s}}{R_s}\langle e^{\chi_s+iS_s}\rangle. \tag{B4}$$

Using Eq. (B1), and taking into account that $(\overline{\chi_s})^2\sim O(\langle\epsilon_{\mathrm{mov}}^4\rangle)$ and $(\overline{S_s})^2\sim O(\langle\epsilon_{\mathrm{mov}}^4\rangle)$ [see Eq. (8)], one obtains from Eq. (B4):

$$\langle p_s\rangle=\frac{e^{ikR_s}}{R_s}\exp\Big(-\frac{1}{2}\langle\chi_s^2\rangle-\frac{1}{2}\langle S_s^2\rangle+i\langle\chi_sS_s\rangle +i\overline{S_s}+O(\langle\epsilon_{\mathrm{mov}}^4\rangle)\Big). \tag{B5}$$

We now compare this equation with Eq. (7.61) from Ref. 4 for the mean sound field calculated by a different approach:

$$\langle p_s\rangle=\frac{e^{ikR_s}}{R_s}\exp\Big(-\frac{1}{2}\langle\chi_s^2\rangle-\frac{1}{2}\langle S_s^2\rangle+O(\langle\epsilon_{\mathrm{mov}}^4\rangle)\Big). \tag{B6}$$

A comparison between Eqs. (B5) and (B6) reveals that

$$\overline{S_s}=-\langle\chi_sS_s\rangle+O(\langle\epsilon_{\mathrm{mov}}^4\rangle). \tag{B7}$$

This formula is also presented in Ref. 3, where it is obtained for a plane wave.

Formulas similar to Eqs. (B3) and (B7) are valid for the wave emitted by the image source

$$\overline{\chi_i}=-\langle\chi_i^2\rangle+O(\langle\epsilon_{\mathrm{mov}}^4\rangle),\quad \overline{S_i}=-\langle\chi_iS_i\rangle+O(\langle\epsilon_{\mathrm{mov}}^4\rangle). \tag{B8}$$

Equations (B3), (B7), and (B8) allow us to calculate the term $\langle e^{\psi_s^*+\psi_i}\rangle$. When calculating this term, we first use Eq. (B1). Then, we replace $\overline{\chi_s}$, $\overline{\chi_i}$, $\overline{S_s}$, and $\overline{S_i}$ by the right-hand sides of Eqs. (B3), (B7), and (B8). The result is

$$\langle e^{\psi_i+\psi_s^*}\rangle=\exp[-\tfrac{1}{2}(\langle\chi_s^2\rangle+\langle S_s^2\rangle+\langle\chi_i^2\rangle+\langle S_i^2\rangle)+\langle\chi_s\chi_i\rangle +\langle S_sS_i\rangle+i(\langle\chi_sS_i\rangle-\langle\chi_iS_s\rangle)+O(\langle\epsilon_{\mathrm{mov}}^4\rangle)]. \tag{B9}$$

The term $\langle e^{\psi_s+\psi_i^*}\rangle$ is a complex conjugation to that $\langle e^{\psi_s^*+\psi_i}\rangle$ and can be obtained from Eq. (B9). Substitution of both terms into Eq. (9) results in Eqs. (10) and (11).

When deriving Eqs. (B9), (10), and (11), one can assume for simplicity that $\overline{S_s}=0$ and $\overline{S_i}=0$. It can be shown that in this case these equations would still hold if the argument of the exponent in Eq. (B9) is augmented by the term $i(\langle\chi_iS_i\rangle-\langle\chi_sS_s\rangle)$, and the argument of cosine in Eq. (10) is added by the term $\langle\chi_iS_i\rangle-\langle\chi_sS_s\rangle$. In this case, Eq. (10) would coincide with the analogous equation from Ref. 1.

APPENDIX C: DERIVATION OF $\langle\chi_s\chi_2\rangle+\langle S_sS_2\rangle$

In Appendix C, we calculate $\langle\chi_s\chi_2\rangle+\langle S_sS_2\rangle$ for the case of anisotropic spectra of temperature and velocity fluctuations.

Expressions for χ_s and χ_2 are given by the real parts of the right-hand sides of Eqs. (16) and (18). Multiplying these expressions and performing ensemble averaging, one obtains

$$\langle \chi_s \chi_2 \rangle = \frac{k^4 L^2}{4^2 \pi^2} \int_0^L dx_1 \int_{-\infty}^{\infty} dy_1 \int_{-h_s}^{\infty} dz_1 \int_{L_1}^{L} dx_2 \int_{-\infty}^{\infty} dy_2 \times \int_{-h_s}^{\infty} dz_2 \frac{B_{\text{eff}}(x_1-x_2, y_1-y_2, z_1-z_2)}{x_1(L-x_1)x_2(L-x_2)} \times \cos\left\{ \frac{kL}{2x_1(L-x_1)} \left[\left(z_1 + (h_s-h_r)\frac{x_1}{L} \right)^2 + y_1^2 \right] \right\} \times \cos\left\{ \frac{kL}{2x_2(L-x_2)} \left[\left(z_2 + 2h_s - (h_s+h_r)\frac{x_2}{L} \right)^2 + y_2^2 \right] \right\}. \tag{C1}$$

Here, $B_{\text{eff}}(x_1-x_2, y_1-y_2, z_1-z_2) = \langle \epsilon_{\text{mov}}(x_1, y_1, z_1) \epsilon_{\text{mov}}(x_2, y_2, z_2) \rangle$ is the correlation function of the random field ϵ_{mov}. We use the Markov approximation for this correlation function: $B_{\text{eff}}(x, \mathbf{r}) = \delta(x) b_{\text{eff}}(\mathbf{r})$. This allows us to calculate the integral over x_2.

Expressions for S_s and S_2 are given by the imaginary parts of the right-hand sides of Eqs. (16) and (18). Therefore, $\langle S_s S_2 \rangle$ is also given by the right side of Eq. (C1) if the two cosines in this equation are replaced by sines. Adding formulas for $\langle \chi_s \chi_2 \rangle$ and $\langle S_s S_2 \rangle$ yields

$$\langle \chi_s \chi_2 \rangle + \langle S_s S_2 \rangle = \frac{k^4 L^2}{4^2 \pi^2} \int_{L_1}^{L} dx \int_{-\infty}^{\infty} dy_1 \int_{-\infty}^{\infty} dy_2 \times \int_{-h_s}^{\infty} dz_1 \int_{-h_s}^{\infty} dz_2 \frac{b_{\text{eff}}(y_1-y_2, z_1-z_2)}{x^2(L-x)^2} \times \cos\left\{ \frac{kL}{2x(L-x)} \left[\left(z_1 + (h_s-h_r)\frac{x}{L} \right)^2 - \left(z_2 + 2h_s - (h_s+h_r)\frac{x}{L} \right)^2 + y_1^2 - y_2^2 \right] \right\}. \tag{C2}$$

In this equation, we introduce new integration variables $u_1 = z_1 + (h_s - h_r)x/L$, and $u_2 = z_2 + 2h_s - (h_s+h_r)x/L$. Equation (C2) becomes

$$\langle \chi_s \chi_2 \rangle + \langle S_s S_2 \rangle = \frac{k^4 L^2}{4^2 \pi^2} \mathrm{Re} \int_{L_1}^{L} dx \int_{-\infty}^{\infty} dy_1 \int_{-\infty}^{\infty} dy_2 \times \int_{m_1}^{\infty} du_1 \int_{-m_2}^{\infty} du_2 \times \frac{b_{\text{eff}}(y_1-y_2, u_1-u_2+2h_s(1-x/L))}{x^2(L-x)^2} \times \exp\left\{ \frac{ikL}{2x(L-x)} [u_1^2 - u_2^2 + y_1^2 - y_2^2] \right\}. \tag{C3}$$

Here, $m_1(x)$ and $m_2(x)$ are given by Eq. (25). Now we introduce new integration variables in Eq. (C3):

$$\xi = u_1 - u_2, \quad \eta = \frac{u_1+u_2}{2}, \quad \xi' = y_1 - y_2, \quad \eta' = \frac{y_1+y_2}{2}. \tag{C4}$$

Then, Eq. (C3) takes the form

$$\langle \chi_s \chi_2 \rangle + \langle S_s S_2 \rangle = \frac{k^4 L^2}{4^2 \pi^2} \mathrm{Re} \int_{L_1}^{L} dx \left\{ \int_{-\infty}^{m_1+m_2} d\xi \int_{m_1 - \xi/2}^{\infty} d\eta + \int_{m_1+m_2}^{\infty} d\xi \int_{-m_2+\xi/2}^{\infty} d\eta \right\} \times \int_{-\infty}^{\infty} d\xi' \int_{-\infty}^{\infty} d\eta' \frac{b_{\text{eff}}(\xi', \xi + 2h_s(1-x/L))}{x^2(L-x)^2} \times \exp\left[\frac{ikL(\xi\eta + \xi'\eta')}{x(L-x)} \right]. \tag{C5}$$

In this equation, the integral over η' is equal to $2\pi\delta(kL\xi'/x(L-x))$. Therefore, the integral over ξ' can be calculated. The result is

$$\langle \chi_s \chi_2 \rangle + \langle S_s S_2 \rangle = \frac{k^3 L}{8\pi} \mathrm{Re} \int_{L_1}^{L} dx \left\{ \int_{-\infty}^{m_1+m_2} d\xi \int_{m_1 - \xi/2}^{\infty} d\eta + \int_{m_1+m_2}^{\infty} d\xi \int_{-m_2+\xi/2}^{\infty} d\eta \right\} \times \frac{b_{\text{eff}}(0, \xi + 2h_s(1-x/L))}{x(L-x)} \exp\left(\frac{ikL\xi\eta}{x(L-x)} \right). \tag{C6}$$

We remind the reader of a useful formula:[1]

$$\int_b^{\infty} d\eta\, e^{ia\eta} = \pi\delta(a) + i\frac{e^{iab}}{a}, \tag{C7}$$

The use of this formula allows us to calculate the integral over η in Eq. (C6). The resulting formula for $\langle \chi_s \chi_2 \rangle + \langle S_s S_2 \rangle$ is given by Eq. (21).

[1] S. F. Clifford and R. J. Lataitis, ''Turbulence effects on acoustic wave propagation over a smooth surface,'' J. Acoust. Soc. Am. **73**, 1545–1550 (1983).

[2] G. A. Daigle, ''Correlation of the phase and amplitude fluctuations between direct and ground-reflected sound,'' J. Acoust. Soc. Am. **68**, 297–302 (1980).

[3] V. I. Tatarskii, *The Effects of the Turbulent Atmosphere on Wave Propagation* (Israel Program for Scientific Translation, Jerusalem, 1971).

[4] V. E. Ostashev, *Acoustics in Moving Inhomogeneous Media* (E & FN SPON, An Imprint of Thompson Professional, London, 1997).

[5] D. K. Wilson and D. W. Thomson, ''Acoustic propagation through anisotropic, surface-layer turbulence,'' J. Acoust. Soc. Am. **96**, 1080–1095 (1994).

[6] Ph. Blanc-Benon, J. Wasier, D. Juvé, and V. E. Ostashev, ''Experimental studies of sound propagation through thermal turbulence near a boundary,'' in *Proceedings of the 29th International Congress and Exhibition on Noise Control Engineering* (Nice, France, 2000).

[7] D. K. Wilson, ''Calculated coherence and extinction of sound waves propagating through anisotropic, shear-induced turbulent velocity fluctuations,'' J. Acoust. Soc. Am. **105**, 658–671 (1999).

[8] P. Chevret, Ph. Blanc-Benon, and D. Juvé, ''A numerical model for sound propagation through a turbulent atmosphere near the ground,'' J. Acoust. Soc. Am. **100**, 3587–3599 (1996).

[9] M. West, K. Gilbert, and R. A. Sack, ''A tutorial on the parabolic equation (PE) model used for long range sound propagation in the atmosphere,'' Appl. Acoust. **37**, 31–49 (1992).
[10] K. E. Gilbert, R. Raspet, and X. Di, ''Calculation of turbulence effects in an upward-retracting atmosphere,'' J. Acoust. Soc. Am. **87**, 2428–2437 (1990).
[11] V. E. Ostashev and G. H. Goedecke, ''Interference of direct and ground reflected waves in a turbulent atmosphere,'' *Proceedings of the 8th International Symposium on Long Range Sound Propagation*, Penn State University, 1998, pp. 313–325.
[12] E. M. Salomons, ''The fluctuating field of a monopole source in a turbulent atmosphere above a ground surface. Time-averaged sound pressure level and statistical distributions,'' in Ref. 11, pp. 326–351.
[13] E. Salomons, V. E. Ostashev, S. Clifford, and R. Lataitis, ''Sound propagation in a turbulent atmosphere near the ground: an approach based on the spectral representation of refractive-index fluctuations,'' J. Acoust. Soc. Am. **109**, 1881–1893 (2001).
[14] K. Attenborough, S. I. Hayek, and J. M. Lawther, ''Propagation of sound above a porous half-space,'' J. Acoust. Soc. Am. **68**, 1493–1501 (1980).
[15] M. A. Nobile and S. I. Hayek, ''Acoustic propagation over an impedance plane,'' J. Acoust. Soc. Am. **78**, 1325–1336 (1985).
[16] X. Di and K. E. Gilbert, ''An exact Laplace transform formulation for a point source above a ground surface,'' J. Acoust. Soc. Am. **93**, 714–720 (1993).
[17] S. M. Rytov, Yu. A. Kravtzov, and V. I. Tatarskii, *Principles of Statistical Radio Physics. Part 4. Wave Propagation Through Random Media* (Springer-Verlag, Berlin, 1989).
[18] A. Ishimaru, *Wave Propagation and Scattering in Random Media* (IEEE Press, New York, 1997).
[19] A. S. Gurvich, A. I. Kon, V. L. Mironov, and S. S. Khmelevtsov, *Laser Radiation in the Turbulent Atmosphere* (Nauka, Moscow, 1976) (in Russian).
[20] Here, we use the following formula: $\lim_{a\to\infty} \sin(a\xi)/\xi = \pi\delta(\xi)$; e.g., see G. A. Korn and T. M. Korn, *Mathematical Handbook* (McGraw-Hill, New York, 1968).
[21] A. V. Kukushkin and I. M. Fuks, ''Reflection formulas for a wave field in a random-nonuniform medium above an ideally reflecting interface,'' Radiophys. Quantum Electron. **31**, 1035–1042 (1980).
[22] V. E. Ostashev, B. Brähler, V. Mellert, and G. H. Goedecke, ''Coherence functions of plane and spherical waves in a turbulent medium with the von Karman spectrum of medium inhomogeneities,'' J. Acoust. Soc. Am. **104**, 727–737 (1998).
[23] J. Mann, ''The spatial structure of neutral atmospheric surface layer turbulence,'' J. Fluid Mech. **273**, 141–168 (1994).
[24] J. Wasier, ''Etude expérimentale des effects d'une frontière sur la propagation des ondes acoustiques à travers une turbulence thermique,'' Ph.D. thesis, ECL 99–46, Ecole Centrale de Lyon, 1999.
[25] Ph. Blanc-Benon and D. Juvé, ''Experimental study of sound propagation above rigid and non rigid boundaries in the presence of turbulence,'' *Proceedings of the 9th International Symposium on Long Range Sound Propagation*, The Hague, 2000 (in press).